Catalysis Science & Technology

Accepted Manuscript

ROYAL SOCIETY OF CHEMISTRY

www.rsc.org/catalysis

Journal Name

ARTICLE

Improved Benzene Production from Methane Dehydroaromatization over Mo/HZSM-5 Catalysts *via* Hydrogen-Permselective Palladium Membrane Reactors†

Received 00th January 20xx,
Accepted 00th January 20xx

DOI: 10.1039/x0xx00000x

www.rsc.org/

S. Natesakhawat,[a,b] N. C. Means,[a,c] B. H. Howard,[a] M. Smith,[d,e] V. Abdelsayed, [d,e] J. P. Baltrus, [a] Y. Cheng,[a] J. W. Lekse,[a,c] D. Link[a] and B. D. Morreale[a]

The effectiveness of hydrogen-permselective palladium membrane reactors for non-oxidative methane dehydroaromatization (MDA) over 4 wt% Mo/HZSM-5 catalysts was investigated as a function of weight hourly space velocity (WHSV) at 700 °C and atmospheric pressure. CH_4 conversion and aromatic product yield decrease with increasing WHSV from 750 to 9000 $cm^3\ g_{cat}^{-1}\ h^{-1}$. C_6H_6 is the main C-containing product at and below 3000 $cm^3\ g_{cat}^{-1}\ h^{-1}$ whereas C_2H_4 dominates the C-product distribution at higher WHSVs. Due to selective removal of H_2 from the reaction products in catalytic membrane reactors, C_6H_6 yield is significantly improved over the whole WHSV range compared to those obtained in fixed-bed reactors. H_2 recovery is strongly influenced by WHSV as it decreases from 48.3% at 750 $cm^3\ g_{cat}^{-1}\ h^{-1}$ to 6.8% at 9000 $cm^3\ g_{cat}^{-1}\ h^{-1}$. There exists a trade-off between catalytic activity and H_2 recovery, which results in the maximum enhancement (~360%) in C_6H_6 yield at 3000 $cm^3\ g_{cat}^{-1}\ h^{-1}$. At this intermediate space velocity, the largest concentration of H_2 is found in the retentate stream and helps alleviate coke accumulation particularly on HZSM-5. Carbon is deposited on the inner surface of the membrane reactor portion in contact with the catalyst bed and transports to the outer surface, thus causing H_2 permeability to decrease over the 15-h reaction period.

Introduction

Efficient conversion of methane to commodity chemicals such as olefins and aromatics is crucial to resolve the environmental, supply, and reliability constraints of using natural gas. Non-oxidative methane dehydroaromatization (MDA) offers a direct route to produce benzene and hydrogen [$6CH_4(g) \leftrightarrow C_6H_6(g) + 9H_2(g)$]. However, the reaction is thermodynamically unfavorable under practical conditions. For example, CH_4 conversion is ~12% and C_6H_6 yield is ~4% at 700 °C and 101 kPa when C(s) is excluded in the calculation of equilibrium composition. Mo/HZSM-5 is the most widely studied catalyst for MDA but readily deactivates due to coke formation. Extensive research has focused on development of Mo/HZSM-5 catalysts using a variety of synthetic techniques and promoters to improve the overall performance in conventional fixed-bed reactors (FBRs). Details on active sites, reaction mechanism, and deactivation of Mo/HZSM-5 catalysts can be found in review papers elsewhere.[1-4]

A promising approach to overcome thermodynamic limitations for this reaction is integration of membrane materials to selectively remove H_2 and drive the reaction toward the formation of C_6H_6. In addition, membrane reactors can improve chemical processes by separating H_2 from other products. Successful applications of membrane processes for H_2 separation have been reported for important industrial reactions such as water-gas shift and methane steam reforming.[5-7] Nevertheless, the use of H_2-permselective membranes for MDA is limited. To date, some of the membrane materials that have been examined include Pd[8], Pd-Ag[9-12], and

[a] National Energy Technology Laboratory, United States Department of Energy, P.O. Box 10940, Pittsburgh, PA 15236, USA
[b] Department of Chemical and Petroleum Engineering, University of Pittsburgh, Pittsburgh, PA 15261, USA
[c] AECOM, 626 Cochrans Mill Road, Pittsburgh, PA 15236, USA
[d] National Energy Technology Laboratory, United States Department of Energy, Morgantown, WV 26507, USA
[e] AECOM, 3610 Collins Ferry Road, Morgantown, WV 26507, USA
E-mail: Sittichai.Natesakhawat@NETL.DOE.GOV; Tel: 1 412 386 5096
†Electronic supplementary information (ESI) available.

dense oxides[13,14]. Information regarding the influence of reaction parameters (*i.e.* feed composition, flow rate, temperature) on H_2 permeation through catalytic membrane reactors (CMRs) under relevant MDA conditions is lacking. While the coupling of conversion and separation processes has proven to enhance CH_4 conversion in some studies, the effect of H_2 removal on product selectivity and yield is largely unknown. Only small improvements in C_2-C_{12} product yields were observed with dense $SrCe_{0.95}Yb_{0.05}O_{3-\delta}$ films.[13] Space velocity is a key design parameter, which influences the reaction/separation performance. Thus, an optimum value of space velocity must be determined to achieve the highest efficiency in membrane operations. In addition, it is unclear whether continuous H_2 removal through membranes adversely affects the catalyst stability by accelerating coking.

In this study, we have synthesized 4 wt% Mo/HZSM-5 catalysts (Si/Al atomic ratio = 25) and evaluated their performance in MDA at 700 °C and atmospheric pressure as a function of weight hourly space velocity (WHSV). These values of the Mo loading and Si/Al atomic ratio were chosen because they have been reported to provide a good balance between active Mo species and Brønsted acid sites in bifunctional Mo/HZSM-5 catalysts to perform the dehydrogenation/ coupling of CH_4 to C_2H_4 and subsequent oligomerization to aromatic products.[15,16] Reaction experiments were conducted in both FBRs and CMRs under the same conditions to determine enhancements in CH_4 conversion and product selectivity/yield. Pd membranes were chosen because they have desirable H_2 flux and selectivity as well as good thermal and mechanical resistance at elevated temperatures. Our previous works have demonstrated that Pd-based membranes exhibited predictable H_2 permeability under the conditions relevant to MDA.[17,18] These properties render Pd-based membranes a potential candidate for integration into the process of CH_4 conversion to C_6H_6 and higher aromatics. Prior to MDA testing, permeation studies were conducted with 125-µm thick unsupported tubular Pd membranes to understand the effects of important process variables such as feed/sweep gas flow rates, H_2 partial pressure, membrane temperature, and presence of CH_4 on H_2 permeation characteristics and mechanical integrity. The catalysts and membranes were characterized before and after MDA to examine the physical, chemical, and structural changes associated with coking using BET surface area and micropore analysis, temperature-programmed hydrogenation/oxidation (TPH/TPO), X-ray photoelectron spectroscopy (XPS), X-ray diffraction (XRD), and scanning electron microscopy with energy dispersive X-ray spectroscopy (SEM/EDS). The goal of the present work is to investigate the influence of WHSV on the effectiveness of Pd membranes for MDA over Mo/HZSM-5 catalysts. In addition, the deactivation behavior of the catalysts is correlated with the differences in MDA performance to shed light on the impact of H_2 removal. A comparison of our results obtained using CMRs to those available in the literature is also presented.

Experimental

Materials

Mo/HZSM-5 catalysts were synthesized *via* incipient wetness impregnation. The nominal Mo loading was fixed at 4 wt%. ZSM-5 zeolite with the Si/Al atomic ratio of 25 was supplied by Zeolyst International in the ammonium form. Initially, HZSM-5 was obtained by calcining NH_4ZSM-5 in flowing air at 500 °C (ramp rate = 2 °C min^{-1}) and holding for 3 h. To prepare 10 g of catalyst, 0.736 g of ammonium heptamolybdate ($(NH_3)_6Mo_7O_{24}{\cdot}4H_2O$, Sigma-Aldrich) and 0.124 g of citric acid (Alfa Aesar) were dissolved in 20 cm^3 deionized water in a heated ultrasonic bath. The mixture was then added dropwise onto 9.6 g of HZSM-5 and the resulting paste was dried overnight at 70 °C. The obtained solid was subsequently calcined in flowing air by ramping to 550 °C (ramp rate = 2 °C min^{-1}) and holding for 4 h. Finally, the powder was pressed and sieved between -20/+60 mesh (particle size range = 250-841 µm). Pd tubular membranes (99.95% purity) were purchased from Goodfellow Corporation with a thickness of 0.125 mm. The membrane tubes were cut to a length of 76.2 mm and mounted to Swagelok unions using graphite ferrules on both ends, thus reducing the remaining exposed length to 46.36 mm (*i.e.* effective membrane area = 9.3 x 10^{-4} m^2). Prior to use, the membrane assemblies were cleaned with acetone and treated under flowing Ar at 700 °C for 3 h in a tube furnace.

Characterization

Elemental analysis of both fresh catalyst and membrane was carried out by Inductively Coupled Plasma-Optical Emission Spectroscopy/Mass Spectrometry (ICP-OES/MS) using a Perkin Elmer Nexion system. A freshly calcined Mo/HZSM-5 catalyst was fused with $LiBO_2$ at 1100 °C and was then digested in 5% HNO_3 with

vigorous stirring. Small chips of a tubular Pd membrane were digested using microwave-assisted aqua regia. The chemical compositions of the fresh catalyst are 5.7 wt% Mo, 2.0 wt% Al, 62.2 wt% Si, which corresponds to the Si/Al atomic ratio of ~30. The ICP analysis confirms a high purity of the as-received membrane, which is 99.95 Pd%. It also contains ppm level of impurities listed in the parentheses as follows: Al (26), Ag (62), Cu (75), Fe (24), Pb (3), Pt (80), and Rh (21).

N_2 adsorption isotherms were performed at 77 K to measure surface area and pore volume of fresh and spent catalysts using a Quantachrome Autosorb 1-C. Prior to measurements, the samples were degassed under vacuum at 300 ^{o}C overnight. Multipoint BET measurements were performed at the relative pressures (P/P_0) in the range of 0.007-0.04 whereas the total pore volumes were measured at $P/P_0 \approx 0.99$. Micropore surface areas and pore volumes were determined using the t-method over the P/P_0 range of 0.15-0.45. TPH/TPO experiments were performed using a Micromeritics Autochem 2950 HP. For TPH, spent catalysts (0.1 g) were heated in flowing 10% H_2/Ar (50 cm^3 min^{-1}) by ramping to 1100 °C (ramp rate = 10 °C min^{-1}) and holding for 30 min. For TPO, spent catalysts (0.1 g) were heated in flowing air (50 cm^3 min^{-1}) with the ramp rate of 10 °C $min^{-1}$to 750 °C. Evolution of CH_4 (*m/z* 16) and CO_2 (*m/z* 44) during TPH and TPO, respectively, was monitored using a Pfeiffer Vacuum Thermostar mass spectrometer.

Fresh and spent Pd membranes were examined using an FEI Company Quanta 600 field-emission scanning electron microscope system that was equipped with secondary and backscatter electron detectors and an Oxford Inca Energy 350 X-act EDS unit. A beam energy of 10 kV was used to examine the surface morphology whereas a beam energy of 20 kV was used for EDS analysis. A small section of the as-received membrane was cut and rinsed with acetone before mounting into the SEM while the spent membrane was analyzed without cleaning. To obtain inner surfaces for analysis, the samples were carefully split in half using surgical scissors to preserve its curvature without introducing superficial surface defects. XRD patterns of fresh and spent materials were obtained with a PANalytical X'Pert Pro MPD diffractometer using Cu K_α radiation (λ = 1.542 Å) operated at 45 kV and 40 mA. XPS was performed using a PHI 5600ci instrument equipped with a monochromatic Al X-ray source (hv = 1486.6 eV) operated at 400 W. The pass energy of the analyzer was set at 58.7 eV. Peak binding energies were referenced to the Si 2p peak located at 103.0 eV.

Apparatus

The tubular reactor system for membrane and catalyst testing was designed and constructed at NETL. A simplified schematic of the reactor system is shown in Fig. 1.

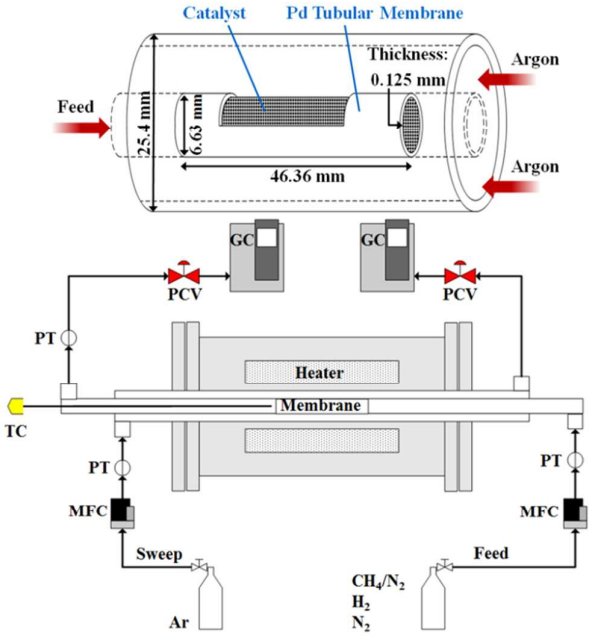

Fig. 1 Schematic of the tubular reactor system for membrane and catalyst testing (GC = gas chromatograph, MFC = mass flow controller, PCV = pressure control valve, PT = pressure transducer, TC = thermocouple)

The reactor assembly consisted of a stainless steel or palladium tube (OD = 6.6 mm, L = 46.4 mm) placed concentrically inside another stainless steel tube (OD = 25.4 mm, L = 990.6 mm). The inner tube (retentate side) was chosen for the feed gas and the outer tube (permeate side) was used for an Ar sweep gas to recover H_2 permeating through the membrane. The direction of gas flow was configured in a counter-current orientation for optimum separation. This experimental apparatus allowed ease of switching operations between FBRs and CMRs. The reactor assembly was heated by a Watlow 120 V, 150 mm long concentric resistance heater which was controlled by a coaxially mounted type-K thermocouple positioned at the bottom of the catalyst bed. All of the gases used were of ultra-high purity grade and their flow rates were controlled by Brooks mass flow controllers. In-line oxygen

traps (Grace) were placed after the mass flow controllers to remove oxygen from both feed and sweep gases to ppb levels. The pressures of the feed and sweep gas streams were regulated by pneumatic, stainless steel control valves from Badger Research and were monitored by pressure transducers from Viatran. The feed and products in the retentate side were analyzed on-line by a Shimadzu GC-2014 gas chromatograph equipped with two flame ionization detectors (FIDs) and a thermal conductivity detector (TCD) using He and Ar as carrier gases, respectively. Separation of the components in the retentate side (N_2, H_2, CO, C_1-C_4, and aromatics) was performed using three columns: Hayesep D (4 m x 1/8 in. SS, 80/100 mesh), molecular sieve 5A (3 m x 1/8 in. SS, 60/80 mesh), and Rtx-5 Amine (30 m x 0.53 mm ID x 3 µm). In the permeate side of the reactor, H_2 was quantified using a second Shimadzu GC-2014 system equipped with a TCD and a molecular sieve 5A column (3 m x 1/8 in. SS, 60/80 mesh). The lines exiting from the reactor to the GCs were heated to 220 °C to avoid product condensation.

Hydrogen permeation measurements

H_2 permeation measurements were conducted under various conditions listed in Table S1 (see the ESI†) to understand the effects of feed/sweep gas flow rates, feed composition, and membrane temperature. For all the experiments, the pressure of the feed gas was kept at 205 kPa while the Ar sweep gas was maintained at 125 kPa. The Pd tubular membrane was filled with 0.5 g of HZSM-5 and packed with quartz wool at both ends. The membrane assembly was pressurized with 308 kPa of air to ensure leak-free connections before loading into the reactor assembly. The system was thoroughly purged at room temperature with flowing Ar at 50 cm^3 min^{-1} for both feed and sweep gas streams. Subsequently, the membrane was heated in flowing Ar at a rate of 10 °C min^{-1} to 350 °C and was held until the temperature was equilibrated. The feed gas was switched from Ar to H_2/N_2 with proper flow rates to achieve the desired concentration.

After the system pressures stabilized, data were taken approximately every 15 min for 2-3 h at each condition. Stability tests were also performed with 10% H_2/N_2 and 10% H_2/CH_4 mixtures at 700 °C for 15 h. This was done in an effort to investigate the effects of CH_4 and coking on the membrane performance.

Catalyst evaluation

MDA over HZSM-5 and Mo/HZSM-5 catalysts was carried out in both FBRs and CMRs at 700 °C. The WHSV was varied between 750 and 9000 cm^3 $g_{cat}^{-1}h^{-1}$ by increasing the feed flow rate from 6.25 to 75 cm^3 min^{-1} while holding the catalyst mass (0.5 g) for each test. For all the measurements with tubular Pd membranes, the Ar sweep gas flow rate was 350 cm^3 min^{-1}. This was found to be the optimum sweep gas flow rate for these tests and will be discussed in more detail later. Prior to reaction, the reactor was purged with 50 cm^3 min^{-1} of Ar while heating step-wise from room temperature to 550 °C (ramp rate = 17 °C min^{-1}) and then to 700 °C (ramp rate = 10 °C min^{-1}) to prevent temperature overshoot. The feed gas was switched from Ar to 90% CH_4-10% N_2 and GC analysis was started. The time on stream (TOS) was set at zero when N_2 was first detected in the product stream at the retentate outlet and the reaction was continued for 15 h. The following definitions were used for describing the catalytic performance in FBRs and CMRs.

$$\%CH_4 \text{ conversion} = \frac{\text{moles of } CH_4 \text{ converted x } 100}{\text{moles of } CH_4 \text{ fed}}$$

$$\%C_6H_6 \text{ yield} = \frac{(6 \text{ x moles of } C_6H_6 \text{ produced}) \text{ x } 100}{\text{moles of } CH_4 \text{ fed}}$$

$$\%H_2 \text{ yield} = \frac{\text{moles of } H_2 \text{ produced x } 100}{(2 \text{ x moles of } CH_4 \text{ fed})}$$

$$\%\mathbf{C_6H_6 \text{ selectivity}} = \frac{(\mathbf{6 \text{ x moles of } C_6H_6 \text{ produced}}) \mathbf{\text{ x } 100}}{\sum(\#\mathbf{C \text{ atoms in C} - \text{product i}}) \, (\mathbf{\text{moles of C} - \text{product i}})}$$

Results and discussion

Hydrogen permeation characteristics

A series of H_2 permeation measurements was conducted on several tubular Pd-membranes packed with HZSM-5 to baseline their performance and elucidate their influence on MDA in CMRs. Specifically, tests were performed to understand the effects of membrane temperature, H_2 partial pressure, and feed/sweep gas flow rates on permeation. Tests were conducted at 350 °C and above to mitigate deleterious effects of H_2 embrittlement (*i.e.* severe lattice strains, distortion, and premature fracture) associated with an α → β hydride phase transition upon cyclic H_2 exposure below 300 °C and 2027 kPa.[19,20] In addition, the permeation study was conducted in the presence of 1-25 mol% H_2/N_2 to encompass

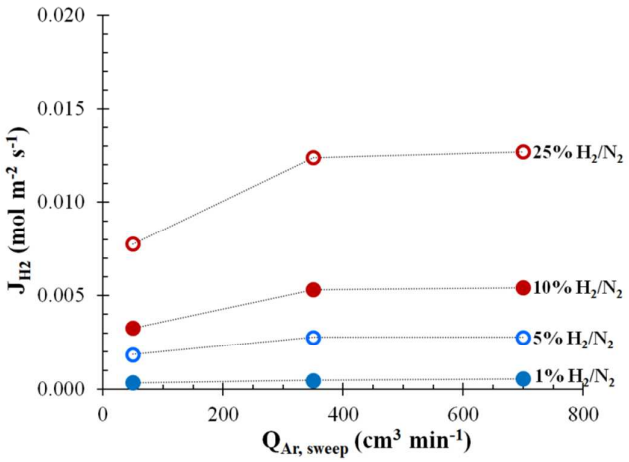

Fig. 2 Effects of the H_2 concentration in the feed and Ar sweep gas flow rate on H_2 permeation flux. Testing conditions are as follows: T = 350 °C, Feed = 1, 5, 10, and 25% H_2/N_2, Q_{Feed} = 50 cm^3 min^{-1}, $Q_{Ar, sweep}$ = 50, 350, and 700 cm^3 min^{-1}.

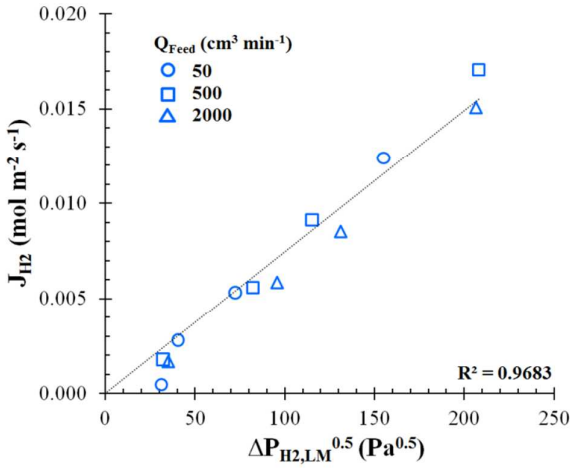

Fig. 3 H_2 permeation flux as a function of the square-root pressure difference for 125-µm thick Pd membranes. Testing conditions are as follows: T = 350 °C, Feed = 1, 5, 10, and 25% H_2/N_2, Q_{Feed} = 50,500, and 2000 cm^3 min^{-1}, $Q_{Ar, sweep}$ = 350 cm^3 min^{-1}. Dotted line is linear regression through the axes origin.

anticipated compositions for evolving H_2 during MDA in CMR experiments.

In order to identify the optimum sweep gas flow rate, permeation measurements were carried out using various H_2/N_2 mixtures with a constant feed flow rate of 50 cm^3 min^{-1} while the Ar sweep flow rate was varied between 50 and 700 cm^3 min^{-1}. When the total pressure of the feed gas was maintained at 205 kPa, a higher H_2 content in the H_2/N_2 mixture yields a higher H_2 partial pressure for permeation. As such, at a constant sweep gas flow rate, H_2 flux increases with the H_2 concentration of the feed from 1% to 25% H_2 (Fig. 2). When the sweep gas flow rate is increased from 50 to 350 cm^3 min^{-1}, the H_2 partial pressure in the permeate side decreases due to dilution of permeated H_2 with Ar, leading to a higher driving force across the membrane. H_2 flux increases more sharply at higher H_2 concentrations in the feed. Upon raising the sweep gas flow rate further to 700 cm^3 min^{-1}, H_2 flux reaches a plateau, which corresponds to the maximum H_2 flux achievable with the membrane. Therefore, the sweep gas flow rate was fixed at 350 cm^3 min^{-1} for subsequent permeation measurements and CMR experiments.

For thick Pd membranes (≥ 10 µm), it is generally assumed that the diffusion of H atoms through bulk Pd is the rate-controlling step for H_2 permeation described by the solution-diffusion mechanism.[21,22] Consequently, H_2 flux can be derived into a Sieverts-type expression as follows:

$$J_{H2} = \frac{k\,(P_{H2,Ret}^{0.5} - P_{H2,Perm}^{0.5})}{\delta}$$

Where J_{H2} is H_2 flux (mol m^{-2} s^{-1}), k is H_2 permeability (mol m^{-1} s^{-1} Pa$^{-0.5}$), $P_{H2,Ret}$ and $P_{H2,Perm}$ are H_2 partial pressure (Pa) in the retentate and permeate sides of the membrane, respectively, and δ is membrane thickness (m). As shown in Fig. 3, H_2 flux is linearly proportional to the log mean difference of the square root of H_2 partial pressure in the retentate and permeate sides, confirming that H_2 flux through the 125-µm thick Pd membranes obeys Sieverts' law under the experimental conditions in this study. A deviation from this law at a very low H_2 flux (a circle point at 31.3 Pa$^{0.5}$) is caused by an experimental error, which is increased with 1% H_2/N_2 due largely to the sensitivity of the GCs and accuracy of the flow meters. Our previous works demonstrated that the H_2 partial pressure exponent in the flux expression deviated from 0.5 to the optimized value ranging between 0.55 and 0.64 at much higher pressures.[17,23] The log mean driving force ($\Delta P_{H2,LM}^{0.5}$) is used to account for the counter-current flow mode.[24] The H_2 permeability at 350 °C calculated from the slope in Fig. 3 is 9.32 x 10^{-9} mol m^{-1} s^{-1} Pa$^{-0.5}$ and is comparable to the values reported for Pd-based membranes tested under similar conditions.[18]

The effect of membrane temperature on H_2 flux was further investigated in 10% H_2/N_2 with the flow rate of 50 cm^3 min^{-1}. This feed gas was chosen because it provided the concentration of H_2 close to the expected maximum value generated in the retentate

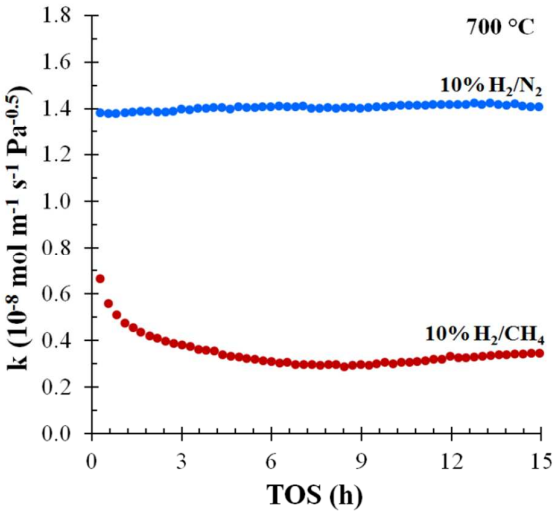

Fig. 4 Apparent H_2 permeability for Pd tubular membranes packed with HZSM-5 as a function of time on stream. Testing conditions are as follows: T = 700 °C, Feed = 10% H_2/N_2 and 10% H_2/CH_4, Q_{Feed} = 50 cm^3 min^{-1}, $Q_{Ar,\ sweep}$ = 350 cm^3 min^{-1}.

side of the CMR during MDA. In a diffusion-limited regime, the apparent activation energy for permeation consists of a contribution from the heat of adsorption (exothermic) and activation energy for diffusion (endothermic).[25] For Pd, the activation energy for diffusion outweighs the heat of H_2 adsorption, resulting in a positive apparent activation energy for permeation.[17,26] As illustrated in Fig. 1S (see the ESI†), H_2 flux increases with temperature from 350 to 450 °C and then reaches a plateau at higher temperatures, indicating that all of H_2 molecules in the feed permeate through the membrane above 450 °C due to the low flow rate and H_2 concentration in the feed used in these tests. Our results are in good agreement with those published in the literature for Pd metal and similar Pd-based membranes in the same temperature range.[26-30]

Poisoning by CH_4 and olefins such as C_2H_4 and C_3H_6 has been reported to hinder H_2 permeation by blocking Pd sites on the membrane surface from adsorbing and dissociating H_2 molecules.[31-33] In addition, these hydrocarbons can further decompose to carbon deposits at elevated temperatures and deteriorate the membrane performance substantially. The effect of CH_4 on H_2 permeation was examined at 700 °C, which is the temperature for MDA testing in both FBRs and CMRs. Apparent H_2 permeability was measured in 10% H_2/CH_4 and was compared to that for 10% H_2/N_2 as a function of TOS displayed in Fig. 4. When N_2 is substituted with CH_4 at 700 °C, the membrane loses up to 75% of H_2 permeability. Under these operating conditions, MDA over HZSM-5 is observed as evidenced by the formation of C_2H_4, C_2H_6, C_3H_6, and trace C_6H_6 detected by the GC. After the permeation testing was completed, there was noticeable discoloration (carbon layer) on the outer surface portion of the membrane that was in contact with the HZSM-5 catalyst bed. Overall, degradation of the Pd membranes during exposure to 10% H_2/CH_4 at 700 °C is attributed to loss of the active membrane surface area from carbon deposits produced during MDA over HZSM-5.

Catalytic measurements in FBRs

Table 1 compares the results obtained with HZSM-5 and 4 wt% Mo/HZSM-5 catalysts for MDA in FBRs at 750 cm^3 g_{cat}^{-1} h^{-1}, which is the lowest value of WHSV achievable in this study. HZSM-5 shows little activity as indicated by low CH_4 conversion and aromatic yield. CO is the main C-containing product observed with HZSM-5. The Mo incorporation into HZSM-5 improves the performance significantly as the Mo/HZSM-5 catalyst exhibits much higher CH_4 conversion, C_6H_6 selectivity, and aromatic yield compared to HZSM-5.

Table 1 Catalytic performance in fixed-bed reactors[a]

Catalyst	CH_4 conversion (%)	Selectivity (%)									Aromatic Yield (%)
		CO	C_2H_4	C_2H_6	C_3H_6	C_6H_6	C_7H_8	C_8H_8	C_8H_{10}	$C_{10}H_8$	
HZSM-5	1.4	64.8	18.1	13.8	0.8	1.9	0.1	0.0	0.0	0.5	0.003
Mo/HZSM-5	7.4	3.4	5.7	3.2	0.3	78.5	5.3	0.1	0.3	3.2	3.9
Mo/HZSM-5 + Pd[b]	5.6	7.5	5.3	6.4	0.3	78.7	1.7	0.0	0.0	0.1	1.5

[a] WHSV = 750 cm^3 g_{cat}^{-1} h^{-1}, TOS = 15 h.
[b] A Pd liner was located inside a fixed-bed reactor.

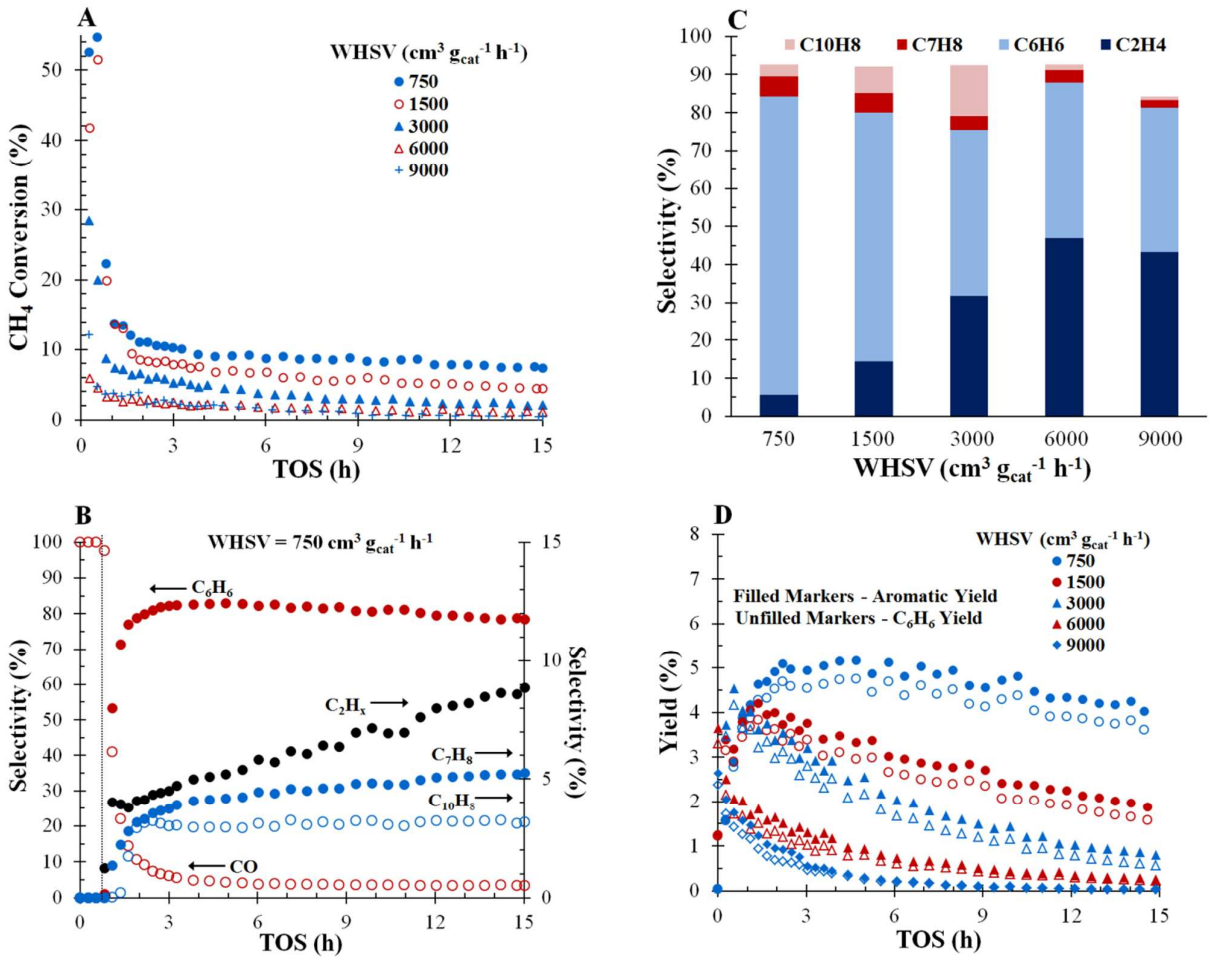

Fig. 5 Effect of WHSV on the performance of the 4% Mo/HZSM-5 catalyst in FBRs (A) CH_4 conversion (B) C-containing product selectivities as a function of TOS at 750 $cm^3\ g_{cat}^{-1}\ h^{-1}$ (C) C-containing product selectivities at TOS = 15 h (D) C_6H_6 and aromatic yields.

These results validate the bifunctional mechanism of MDA over Mo/HZSM-5 catalysts where active Mo carbide species activate CH_4 to C_2 hydrocarbons as the primary intermediates (mainly C_2H_4) and Brønsted acid sites in HZSM-5 subsequently oligomerize these intermediates to C_6H_6 and heavier aromatics.[1,4] The presence of a Pd liner located inside an FBR (*i.e.* no H_2 permeation was allowed) negatively affects the performance of the Mo/HZSM-5 catalyst. An increase in C_2H_6 selectivity is attributed to the coupling of CH_4 to C_2H_6 on the Pd liner, which competes with the dehydrogenation of CH_4 to C_2H_4 over the Mo/HZSM-5 catalyst. At TOS = 15 h, the formation rate of C_2H_4 decreases from 40 to 15 µmol $g_{cat}^{-1}\ h^{-1}$ when the Pd liner is placed inside the FBR. Therefore, the yield of the aromatic compounds is noticeably suppressed.

The effect of WHSV on the performance of the 4 wt% Mo/HZSM-5 catalysts in MDA was examined. Prior to reaction, the catalyst was not activated *in situ* so that an induction period could be monitored. As shown in Fig. 5A, CH_4 conversion decreases with increasing WHSV due to shorter residence time in the reactor at high WHSVs. At TOS = 15 h, CH_4 conversion is 7.4% at 750 $cm^3\ g_{cat}^{-1}\ h^{-1}$ and it decreases to 0.4% at 9000 $cm^3\ g_{cat}^{-1}\ h^{-1}$. The induction period can only be seen at low WHSVs where CH_4 conversion reaches a maximum in the early stage of the reaction. The induction period is considerably shortened or completely eliminated at and above 3000 $cm^3\ g_{cat}^{-1}\ h^{-1}$ and it cannot be observed because the reaction data were taken every ~15 min. Regardless of WHSV, CH_4 conversion decreases steeply during the first 3 h due to rapid formation of carbon deposits on the catalyst and the activity gradually declines for the remaining TOS.

Fig. 5B illustrates the selectivity to primary C-containing products as a function of TOS at 750 cm^3 g_{cat}^{-1} h^{-1}. The induction period is clearly seen, which corresponds to the amount of time before the formation of the aromatic compounds (approximately 1 h, dashed line).[34] During the induction period, CH_4 reduces and carburizes MoO_x species in the catalyst to form active MoO_xC_y and/or Mo_2C.[35-37] An observation of the induction period is consistent with the concurrent evolution of CO with 100% selectivity. Consequently, high CH_4 conversion (Fig. 5A) during the first hour of the reaction is due to the reduction of MoO_x species by CH_4 in the feed gas.[38] As soon as the induction period is complete, C_2 hydrocarbons (mostly C_2H_4 and C_2H_6) and trace aromatics (C_6H_6, C_7H_8) start appearing while CO selectivity dramatically falls to 41.1% at this stage. $C_{10}H_8$ appears shortly after the formation of C_6H_6, suggesting that $C_{10}H_8$ is produced after successive alkylation of C_6H_6 by the C_2 intermediates.[39] After 5 h, C_6H_6 selectivity reaches a maximum (82.9%) and then decreases steadily whereas the selectivity to C_7H_8 and $C_{10}H_8$ increases very slowly at longer TOS. On the other hand, C_2 selectivity continues to increase, signaling that carbon deposition deactivates the Brønsted acid sites in the zeolite channels where the C_2 intermediates undergo oligomerization and cyclization to form the aromatic products.[34]

The variation of the selectivity to the main C-containing products with WHSV is presented in Fig. 5C. As WHSV is increased, the selectivity to C_6H_6 and C_7H_8 decreases while C_2H_4 selectivity increases. High CH_4 conversion achieved at low WHSVs is accompanied by large accumulation of coke particularly inside the zeolite channels, which decreases their effective diameter and in turn inhibits the formation and diffusion of bulky $C_{10}H_8$ molecules.[38,40] For this reason, $C_{10}H_8$ selectivity increases with WHSV and reaches a maximum at 3000 cm^3 g_{cat}^{-1} h^{-1}. C_6H_6 dominates the distribution of C-containing products between 750 and 3000 cm^3 g_{cat}^{-1} h^{-1}, where its selectivity ranges from 43.8 to 78.5%. At higher WHSVs, the oligomerization of the C_2 intermediates (a secondary reaction) in HZSM-5 is minimized due to shorter residence time. Thus, C_2H_4 becomes the main C-containing product at and above 6000 cm^3 g_{cat}^{-1} h^{-1}. Furthermore, C_6H_6 and aromatic yields decrease as WHSV is increased and they gradually decline with TOS (Fig. 5D). At higher WHSVs, the formation of C_6H_6 is more favorable than that of the heavier aromatics and therefore the difference between the aromatic and C_6H_6 yields is less evident.

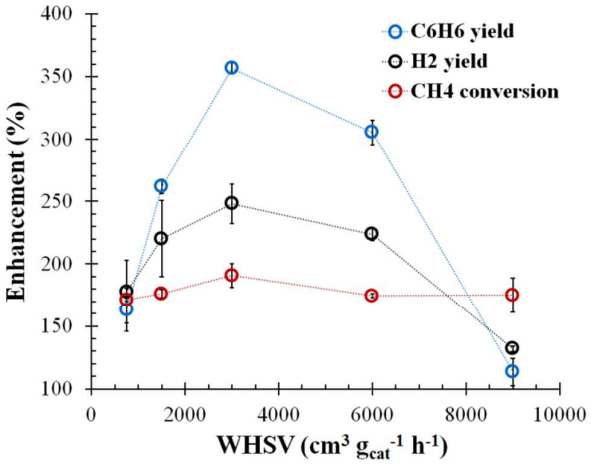

Fig. 6 Effect of WHSV on the performance enhancement in CMRs at TOS = 15 h.

Overall, our results are comparable to the literature values obtained with various Mo/HZSM-5 catalysts under similar MDA conditions.[41-45]

Enhanced performance in CMRs

To evaluate the benefits of employing Pd membranes, MDA was also carried out over the 4 wt% Mo/HZSM-5 catalyst in CMRs under the same WHSV range at 700 °C. The results are compared to those from FBRs in terms of enhancement, which is defined as the ratio of CH_4 conversion (or product yield) achieved by a CMR to that by an FBR at TOS = 15 h (Fig. 6). For the CMR experiments, H_2 yield is calculated from the total amount of H_2 generated in both retentate and permeate sides. CH_4 conversion and product yields are higher in the CMRs than in the FBRs for the whole range of WHSV examined. Among the three parameters, C_6H_6 yield is the most improved. WHSV plays an important role in the effectiveness of the Pd membrane for H_2 separation during MDA as the enhancement is maximized at 3000 cm^3 g_{cat}^{-1} h^{-1}. It is worth noting that external mass transfer effects can be neglected under these testing conditions, which was confirmed by the Mears criterion calculations (see the ESI†).

A representative comparison of the catalytic performance in both reactors is shown in Fig. 2S (see the ESI†) for the entire TOS at 3000 cm^3 g_{cat}^{-1} h^{-1}. *In situ* removal of H_2 can alleviate thermodynamic constraints by shifting the equilibrium toward the product side, leading to increased CH_4 conversion and aromatic yield. However, CH_4 conversion achieved by the CMR is still well

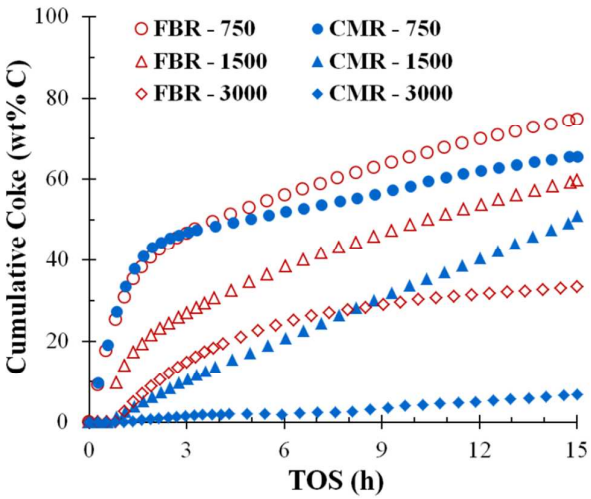

Fig. 7 Effect of WHSV on cumulative coke formation in FBRs and CMRs.

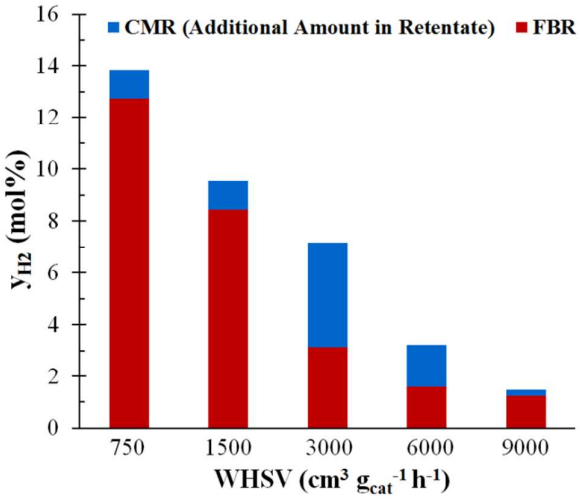

Fig. 8 Comparison of H_2 concentration of the product stream (or retentate outlet) in the FBRs and CMRs at different WHSVs.

below the equilibrium conversion under these conditions (~12%). C_6H_6 yield achieved by the CMR at TOS = 15 h is 2.05% compared to 0.57% by the FBR, which corresponds to the highest value of enhancement (~360%). Furthermore, $C_{10}H_8$ selectivity is markedly suppressed in the CMR (*i.e.* from 13.4% to 3.0%).

Under typical operating conditions, carbon deposition is inevitable and it causes the activity loss of Mo/HZSM-5 catalysts as illustrated in Fig. 5 and 2S. Mechanistically, the main deactivation process involves adsorption and condensation of heavy aromatic compounds such as $C_{10}H_8$, which are coke precursors, on the Brønsted acid sites located on the external surface of HZSM-5.[46] As coke accumulates, partial and extensive steric blockage of the zeolite channels by exterior deposits are very likely.[47] Fig. 7 compares the cumulative coke formation in the CMRs to that in the FBRs. Coke accumulates over reaction time and coke formation is enhanced at low WHSVs. The accumulation of coke is minimized in the CMRs and it is remedied to a larger extent at 3000 cm^3 g_{cat}^{-1} h^{-1} as the coke content in the CMR is 6.9 wt% compared to 33.3 wt% in the FBR at TOS = 15 h.

The addition of H_2 (up to 9 mol%) to the CH_4 feed was reported to minimize carbon deposition during MDA over Mo/HZSM-5 catalysts by hindering the formation of heavy aromatics and their adsorption on the Brønsted acid sites of the zeolites.[48-50] The use of H_2 regeneration cycles was also found to partially remove coke deposits on similar catalysts.[11,51,52] Hagen *et al.* proposed that H_2 may suppress coking *via* scission of fragments from coke precursors such as olefinic oligomers formed inside the zeolite channels.[53]

Accordingly, an excess amount of H_2 generated in the retentate side of a CMR would help restrain catalyst deactivation by coke formation. Fig. 8 compares the concentration of H_2 in the reaction mixture exiting the FBRs and CMRs as a function of WHSV at TOS = 15 h. H_2 production decreases at high WHSVs owing to low CH_4 conversion. An increased concentration of H_2 in the retentate side of the CMR is most pronounced at 3000 cm^3 g_{cat}^{-1} h^{-1}. The additional amount of H_2 in the CMR is effective in suppressing coke accumulation during MDA, thereby enhancing the formation of C_6H_6. This finding agrees very well with the observed trend for the enhancement of C_6H_6 yield which is maximized at 3000 cm^3 g_{cat}^{-1} h^{-1} (Fig. 6) and improved resistance to coking of the Mo/HZSM-5 catalyst in the CMRs at the same space velocity (Fig. 7).

The Pd membranes were examined to monitor changes in surface morphology and chemical composition. Fig. 9 shows SEM images with different magnifications for both outer (permeate side) and inner (retentate side) surfaces of the fresh and spent membranes along with elemental analysis by EDS. For each sample, multiple locations were analyzed to check for variations in composition by EDS but only one representative spot is shown for brevity. The morphology of the outer surface of the as-received membrane is uniform with visible grooves probably resulting from the fabrication technique for manufacturing tubular Pd membranes (Fig. 9A). The inner surface of the same membrane displays irregular-shaped Pd grains with varying sizes less than 100 µm (Fig. 9B). EDS analysis for both surfaces of the as-received sample indicates a very high concentration of Pd, which agrees very well

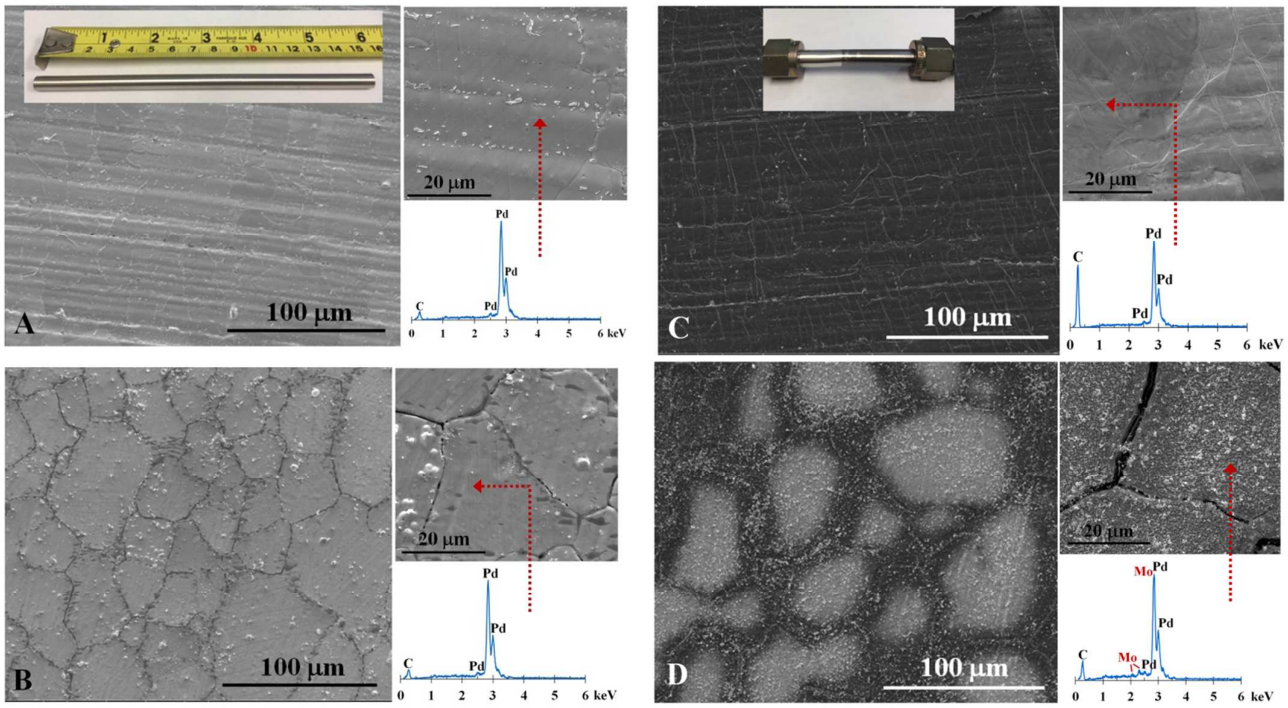

Fig. 9 SEM micrographs (with different magnifications) and corresponding EDS analysis (A) outer, as-received (B) inner, as-received (C) outer, spent (D) inner, spent. Insets show photographs of the outer surface of the fresh and spent membranes (WHSV = 3000 $cm^3\ g_{cat}^{-1}\ h^{-1}$, TOS = 15 h).

with the ICP results. Carbon is likely due to surface residues. A photograph of the spent Pd tube (Fig. 9C, inset) illustrates visible discoloration on the outer surface along the portion where the Mo/HZSM-5 catalyst was in contact with the inner surface. SEM analysis verifies that the dark region is ascribed to filamentous carbon deposits on the outer surface of the spent membrane (Fig. 9C). It appears that carbon originated from the inner surface of the membrane during MDA and then migrated through the Pd lattice to the outer surface. No pinholes or swelling was observed with the spent membrane. However, the Pd grains appear to grow larger upon heating to 700 °C and carbon preferentially accumulates near the grain boundaries (Fig. 9D). Consistently, the EDS analysis of surface sites of the spent membrane shows a pronounced increase in the C signal. Residual catalyst was also seen on the inner surface of the spent membrane as suggested by the Mo signal.

H_2 recovery is an important indicator of the membrane performance and corresponds to the amount of H_2 recovered through the membrane with respect to the total H_2 production.[54,55] H_2 recovery is expressed as follows:

$$\%H_2\ \text{recovery} = \frac{Q_{H2,Perm}\ x\ 100}{(Q_{H2,Ret} + Q_{H2,Perm})}$$

Where $Q_{H2,Ret}$ and $Q_{H2,Perm}$ are H_2 molar flow rate in the retentate and permeate sides of the membrane, respectively. As illustrated in Fig. 10A, H_2 recovery decreases with increasing WHSV. This finding is attributed to low H_2 partial pressure in the retentate side at high WHSVs, which in turn diminishes H_2 flux or a driving force for permeation through the membrane. Consistently, H_2 permeability decreases when WHSV is increased. Due to carbon deposition on the inner and outer surfaces of the membrane as evidenced by SEM-EDS results in Fig. 9, the membrane packed with the Mo/HZSM-5 catalyst continues to lose its permeability over time. As displayed in Fig. 10B, the loss of H_2 permeability is more noticeable compared to that previously seen with the HZSM5-packed membrane examined during the permeation testing at 700 °C (Fig. 4). Under certain operating conditions, continuous H_2 removal over the course of the reaction can affect the catalyst stability by enhancing the carbon deposition rate, leading to widening of the carbon formation zone.[54] At low WHSVs, high activity is offset by high H_2 recovery, which leads to less H_2 available

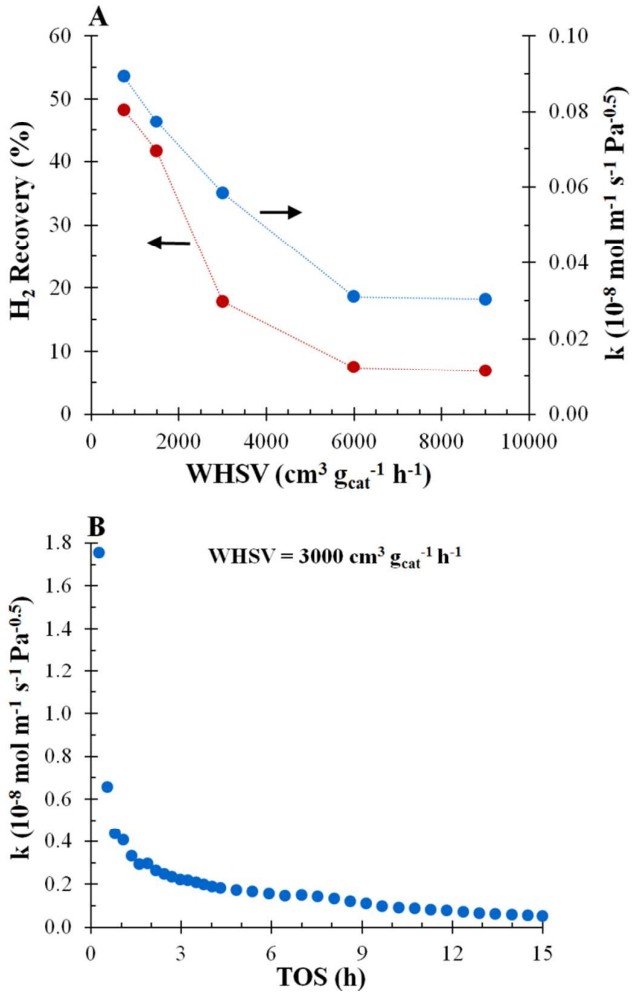

Fig. 10 (A) H_2 recovery and apparent permeability as a function of WHSV (TOS = 15 h) (B) H_2 permeability as a function of TOS at 3000 $cm^3\ g_{cat}^{-1}\ h^{-1}$.

for catalyst regeneration in the retentate side of the CMR. We have demonstrated that the optimum WHSV for the CMR experiments is 3000 $cm^3\ g_{cat}^{-1}\ h^{-1}$ (Fig. 6). Therefore, the largest enhancement of C_6H_6 yield achieved in this study is a result of a trade-off between catalytic activity and H_2 recovery where coking is kept to a minimum at this intermediate space velocity.

According to our XPS analysis, spent samples collected from both FBR and CMR exhibit very similar surface characteristics with regard to atomic concentrations and binding energies of all the elements constituting the catalyst. For this reason, the representative XPS results for the spent CMR sample only are shown here. At 700 °C, isolated MoO_x species can further diffuse into the channels of HZSM-5 and anchor at cation exchange sites by replacing protons.[16,56] A decrease in the atomic Mo/Al and Mo/Si ratios (Table 2) demonstrates that most of the Mo species in the spent catalyst indeed migrate into the zeolite channels during catalysis. For the fresh sample, the binding energy of the Mo $3d_{5/2}$ peak in Fig. 11A is 232.8 eV, which is indicative of Mo^{6+} species.[40,57] Mo exists in multiple oxidation states on the surface of the spent sample. The Mo 3d peak envelope was resolved into the components with Mo $3d_{5/2}$ binding energies as follows: 232.7 eV (Mo^{6+}), 231.0 eV (Mo^{5+}), and 228.6 eV (Mo^{4+}). These results show that the majority of the surface Mo species in the spent catalyst are in the 4+ oxidation state (46.7%) with the remaining 11.8% and 41.6% occurring as Mo^{5+} and Mo^{6+}, respectively. CO was detected for the whole test period regardless of WHSV (for example, Fig. 5B),suggesting that MoO_x species particularly those associated with the Brønsted acid sites are not completely reduced and carburized to Mo_2C.[45,58] It is very likely that MoO_xC_y originates from the reduction of $(Mo_2O_5)^{2+}$ dimers by CH_4.[59,60] Because the Mo $3d_{5/2}$ binding energy for MoO_xC_y and Mo_2C (*i.e.* 227.6-228.6 eV)[40,57,61] is very close to that for Mo^{4+}, it may be difficult to distinguish these species. The C 1s spectra are usually employed to verify the presence of carbide associated with Mo as its C 1s binding energy is typically reported to be between 282.7 and 283.9 eV.[40] Fig. 11B illustrates that graphitic carbon at 284.3 eV is the predominant carbon species detectable on the catalyst surface.[40,62,63] The C1s peak grows much larger after MDA, which is attributed to coking in the spent catalyst (Table 2). Based on the C1s spectra, it appears that Mo_2C is not present on the catalyst surface. However, we cannot completely rule out that a trace amount of Mo_2C may be present in the spent sample because any carbide associated with the small quantity of surface Mo may be obscured by the high relative intensity of the C1s peak due to graphitic carbon. After 15 h TOS, the catalyst surface could be covered by multiple layers of coke.[64]

Table 2 Surface compositions of fresh and spent Mo/HZSM-5 catalysts (WHSV = 3000 $cm^3\ g_{cat}^{-1}\ h^{-1}$, TOS = 15 h) determined by XPS analysis

Catalyst	Concentration (at%)					Mo/Al	Mo/Si
	C 1s	O 1s	Si 2p	Al 2p	Mo 3d		
Fresh	6.7	63.2	27.3	0.8	1.9	2.375	0.070
Spent	62.5	23.1	13.1	0.7	0.6	0.871	0.047

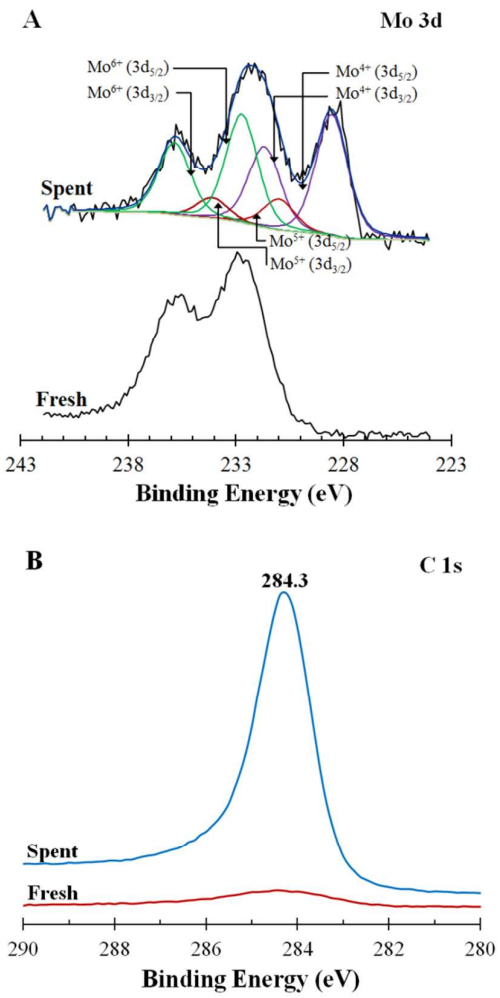

Fig. 11 XPS results for fresh and spent catalysts (A) Mo 3d (B) C 1s.

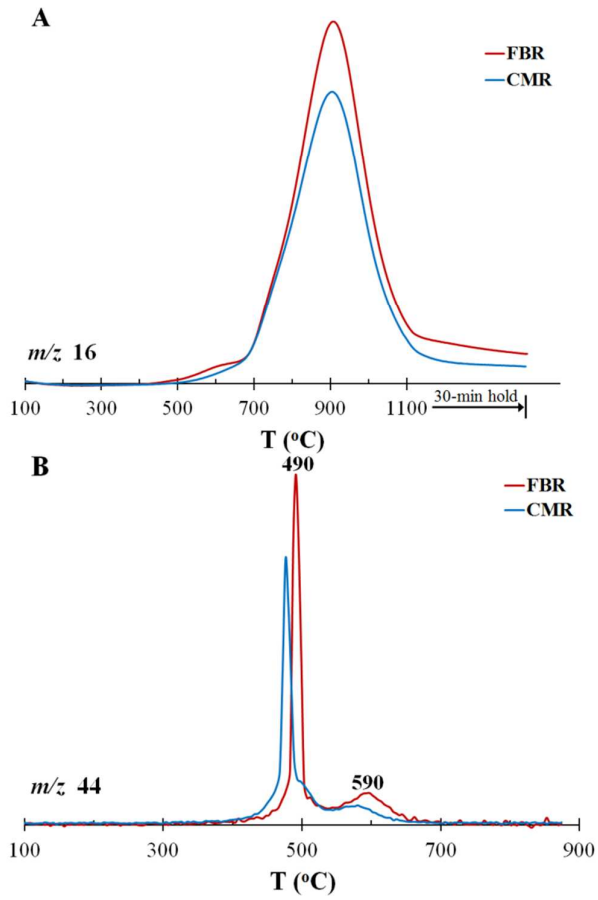

Fig. 12 Profiles for the spent catalysts collected from the FBR and CMR operated at 3000 $cm^3\ g_{cat}^{-1}\ h^{-1}$: (A) TPH (B) TPO

As a result, XPS is unable to probe the depths at which carbidic carbon in Mo carbides is formed. In addition, we cannot overlook the possible instability of the carbide phase that is exposed to air prior to XPS analysis.[65] Our results are in good agreement with those reported by Fadeeva *et al.*[66] that a significant amount of Mo^{6+} species was detected on the surface of a similar catalyst after CH_4 exposure at 700 °C and the formation of surface Mo_2C could not be confirmed by XPS.

It is believed that coke formed on the Brønsted acid sites of HZSM-5 is responsible for pore blocking and catalyst deactivation.[46] The characteristics of carbon deposits on the spent catalysts collected after 3000 $cm^3\ g_{cat}^{-1}\ h^{-1}$ testing from both FBR and CMR were evaluated by TPH/TPO. As shown in Fig. 12A, the TPH profiles demonstrate that carbon deposits on the spent catalysts can be hydrogenated to form CH_4 (*m/z* 16) starting at ~450 °C. However, hydrogenation of less reactive coke such as graphitic would require high temperature.[67] Carbon deposits can be more easily combusted by air as the evolution of CO_2 (*m/z* 44) during TPO is complete at a lower temperature (Fig. 12B). The TPO profile of the spent FBR sample exhibits a sharp feature at 490°C, which has been assigned to carbon in Mo carbides and Mo-associated coke.[64,68-70] The high-temperature feature around 590 °C is attributed to aromatic-type carbon deposits mostly on the Brønsted acid sites in the zeolite channels.[64,71] The TPO profiles for the spent samples are typically the bifunctional nature of Mo catalysts supported on zeolites.[64,72] Tessonnier *et al.* pointed out that extraframework Al species located at the pore mouth of HZSM-5 were important coke generators.[16] As such, oxidation of coke formed on those species at the external surfaces of the zeolite may also contribute to the high-temperature peak observed in the TPO profiles. A lower intensity of the CO_2 signal seen with the spent CMR sample corroborates that

Table 3 Textural properties of Mo/HZSM-5 catalysts

Catalyst[a]	S_{BET} ($m^2 g^{-1}$)	S_{Micro} ($m^2 g^{-1}$)	V_{total} ($cm^3 g^{-1}$)	V_{Micro} ($cm^3 g^{-1}$)	V_{Micro} loss (%)
Fresh	356	260	0.774	0.107	-
Spent, CMR	236	186	0.560	0.073	32
Spent, FBR	144	101	0.400	0.040	63

[a] Spent catalysts were collected after 15 h-reaction (WHSV = 3000 $cm^3 g_{cat}^{-1} h^{-1}$).

coking is suppressed by an additional amount of H_2 generated in the CMR (Fig. 8). Our TPH/TPO observations agree well with the finding of Kojima *et al.*[49] that H_2 addition in the CH_4 feed efficiently removed carbon deposits on the Brønsted acid sites of HZSM-5 *via* hydrogenation facilitated by the presence of precious metal promoters such as Pt and Rh in the catalysts.

Accumulation of coke at the pore mouths and/or within the pores of HZSM-5 decreases micropore surface area and volume, thus making the Brønsted acid sites inaccessible for the formation of C_6H_6 and higher aromatics.[73] Both spent FBR and CMR samples exhibit loss of micropore surface area and pore volume (Table 3). However, the spent CMR sample provides a smaller decrease in micropore volume (32%) in comparison to that of a fresh catalyst. The results from TPH/TPO and micropore measurements are in accordance with less coke accumulation and enhanced performance observed with the catalysts in the CMRs.

The crystallinity and crystal structure of both fresh and spent materials were examined by XRD and their corresponding patterns are compared in Fig. 3S (see the ESI†). The pattern of the parent zeolite shows characteristic peaks of a crystalline ZSM-5 structure (JCPDS# 00-042-0024). The crystal structure of HZSM-5 is preserved upon the Mo incorporation and remains intact after MDA testing. There are no detectable peaks associated with crystalline Mo-containing species in the Mo/HZSM-5 catalysts, suggesting that Mo is either well-dispersed or is incorporated into the zeolite channels. Furthermore, bulk crystalline Pd in the fresh membrane exhibits a cubic structure (JCPDS# 00-046-1043) as confirmed by the appearance of the (111), (200), and (220) peaks at 2θ = 40.1°, 46.6°, and 68.1°, respectively. Graphitic carbon (JCPDS# 00-041-1487) is detected with both inner and outer surfaces of the spent membrane but most resides on the inner surface. These XRD results coupled with the SEM-EDS findings provide concrete evidence of carbon deposition on the membrane surfaces that contributes to performance degradation of the Pd membranes during MDA testing.

Comparison to published CMR data

Table 4 summarizes the results available in the literature for MDA in CMRs.[8-14,74] However, a direct, quantitative comparison is not possible due to the differences in catalyst (composition, preparation conditions), membrane (material, thickness, effective area, configuration) and operating conditions (feed composition, temperature, WHSV, TOS, sweep gas, etc.) used by different authors. As a general consideration, H_2-permselective Pd-based membranes were the most utilized with the main goal of improving CH_4 conversion compared to conventional FBRs between 500 and 700 °C. Operations at low temperatures enhanced CH_4 conversion beyond thermodynamic equilibrium levels.[9,74] There is no consensus on the optimum WHSV to achieve the highest C_6H_6 and aromatic yields. Most of the early studies were conducted at very low WHSVs (*i.e.* below 780 $cm^3 g_{cat}^{-1} h^{-1}$). It is possible that these space velocities were chosen to maximize H_2 removal, thus shifting the equilibrium as far as possible toward the product side. Wang *et al.*[9] and Iliuta *et al.* [74] demonstrated that CH_4 conversion in the CMRs improved with decreasing WHSV and the enhancement was most evident around 120-130 $cm^3 g_{cat}^{-1} h^{-1}$. On the other hand, we have demonstrated that the activity enhancement particularly in C_6H_6 yield exhibits a volcano-shaped curve with a maximum at 3000 $cm^3 g_{cat}^{-1} h^{-1}$ (Fig. 6).

Besides improvements in CH_4 conversion, changes in product distribution induced by CMRs were overlooked in many studies. Another important parameter which most researchers did not take into account when describing the membrane effect on the separation process is H_2 recovery. Consequently, the effectiveness of the membrane for MDA cannot be fully evaluated and then correlated with increased CH_4 conversion. Information about key membrane characteristics (*i.e.* effective area, thickness) and how the operating conditions affect H_2 permeability is scarce. We find that coke accumulation can be suppressed for some extent without the presence of O_2 or steam in the CH_4 feed when there is a sufficient amount of H_2 remaining in the retentate side. On the contrary, Iliuta *et al.*[74] and Rival *et al.*[10] reported that coking was accelerated in the CMRs operated at low WHSVs and under vacuum

Table 4 Comparison to literature results for MDA in catalytic membrane reactors

Authors	Membrane	Mo loading (wt%)	Si/Al	T (°C)	WHSV ($cm^3\ g_{cat}^{-1}\ h^{-1}$)	TOS (h)	Sweep gas[f]	CH_4 conversion[h] (%) @ equilibrium	CH_4 conversion[h] (%) max.	Enhancement[i] (%)
This work	Pd	4	25	700	750-9000	15	Ar (350)	12.3	12.7 (750)	191 (3000)
Cao *et al.*[14,a]	$Ba_{0.5}Sr_{0.5}Co_{0.8}Fe_{0.2}O_{3-\delta}$ (BSCF)	6	27	750	6000	17	Air (30)	17.3	10.5	140
Kinage *et al.*[8,b]	Pd	3	NA	610	290	100	N_2	3.3	3.5	NA
Liu *et al.*[13,c]	$SrCe_{0.95}Yb_{0.05}O_{3-\delta}$	4	15	677-720	780	20	He	10.4-14.5	13.5	145
Iliuta *et al.*[12,d]	Pd-Ag	3	15	600-700	270	10	None[g]	5.5-12.3	14.0	140
Iliuta *et al.*[74,d]	Pd-coated Ta/Nb	3	15	600	130-770	24	None[g]	5.5	13.0 (130)	310 (130)
Larachi *et al.*[11,d]	Pd-Ag	3	15	600-700	270	9	None[g]	5.5-12.3	16.0	160
Rival *et al.*[10,d]	Pd-Ag	3	15	500-600	270-770	10	None[g]	2.0-5.5	2.5	NA
Wang *et al.*[9,e]	Pd-Ag	NA	NA	585	120-1440	6	None[g]	4.8	7.5	300

NA = Not available.
[a] Oxidative reaction atmosphere with air in the permeate side.
[b] Reaction pressure was 5 atm.
[c] The CH_4 feed contained 2% CO_2.
[d] The Mo/HZSM-5 catalyst was promoted with 0.5 wt% Ru.
[e] Both Mo/HZSM-5 and Re/HZSM-5 catalysts were evaluated.
[f] The number in the parentheses indicates the flow rate in $cm^3\ min^{-1}$.
[g] Permeated H_2 was removed by a vacuum pump.
[h] The number in the parentheses for the maximum conversion indicates WHSV.
[i] Maximum enhancement was calculated from CH_4 conversion. The number in the parentheses indicates WHSV.

conditions. This discrepancy may be associated with a lack of H_2 in the retentate side needed for hydrogenating carbon species formed on the catalysts.[11] More recently, oxidative MDA was attempted to suppress coking by using an O_2-permeable perovskite membrane to continuously feed O_2 to generate steam in the retentate side *via* selective combustion ($6CH_4 + 9/2\ O_2 \rightarrow C_6H_6 + 9H_2O$).[14] Carbon oxides became the primary C-containing products since partial or total oxidation of CH_4 was more favorable than MDA. Although the selectivity and yield of the aromatic compounds declined sharply, the Mo/HZSM-5 catalyst was more resistant to coking while remaining in an active carbide state upon O_2 exposure. Finally, our results indicate that a marked improvement in CH_4 conversion and C_6H_6 yield/selectivity can be achieved in CMRs even though H_2 permeability deteriorates to a large extent due to carbon deposition on both inner and outer surfaces of the Pd membranes.

Conclusions

This study has demonstrated the advantages of using tubular Pd membranes packed with Mo/HZSM-5 catalysts for non-oxidative MDA over a wide range of space velocities at 700 °C. Although *in situ* H_2 removal does not overcome the thermodynamic equilibrium limitations under the experimental conditions, a significant improvement with regard to CH_4 conversion and total aromatic yield can be observed in comparison to those achieved in conventional FBRs. Specifically, C_6H_6 yield enhancement is strongly correlated with WHSV and it is maximized at 3000 $cm^3\ g_{cat}^{-1}\ h^{-1}$. An additional amount of H_2 generated in the retentate side of the CMR inhibits coke accumulation on the catalysts, thereby enhancing C_6H_6 formation. Our results are the first to demonstrate a balance between catalytic activity and H_2 recovery at this intermediate space velocity, which contributes to the observed maximum enhancements in MDA. Permeation testing with 125-μm thick tubular Pd membranes has demonstrated that H_2 flux measured in 1-25 mol% H_2/N_2 mixtures follows Sieverts' law as it is found to be linearly proportional to the difference of the square root of H_2 partial pressure in the retentate and permeate sides (*i.e.* $J_{H2} \propto$

$[P_{H2,Ret}^{0.5}-P_{H2,Perm}^{0.5}]$). H_2 permeability of the Pd membranes degrades over time owing to carbon deposition on both inner (retentate side) and outer (permeate side) surfaces under MDA conditions. However, these membranes do not show any sign of leakage or swelling after 15 h of operation, suggesting that they could have potential for practical applications in the conversion of CH_4 to chemicals and liquid fuels.

Acknowledgements

This project was funded by the Department of Energy, National Energy Technology Laboratory, an agency of the United States Government, through a support contract with AECOM Energy &Construction, Inc. Neither the United States Government nor any agency thereof, nor any of their employees, nor AECOM Energy & Construction, Inc., nor any of their employees, makes any warranty, expressed or implied, or assumes any legal liability or responsibility for the accuracy, completeness, or usefulness of any information, apparatus, product, or process disclosed, or represents that its use would not infringe privately owned rights. Reference herein to any specific commercial product, process, or service by trade name, trademark, manufacturer, or otherwise, does not necessarily constitute or imply its endorsement, recommendation, or favoring by the United States Government or any agency thereof. The views and opinions of authors expressed herein do not necessarily state or reflect those of the United States Government or any agency thereof.

Notes and references

1 Z.R. Ismagilov, E.V. Matus, L.T. Tsikoza, *Energy Environ. Sci.*, 2008, **1**, 526-541.
2 S. Majhi, P. Mohanty, H. Wang, K.K. Pant, *J. Energy Chem.*, 2013, **22**, 543-554.
3 S. Ma, X. Guo, L. Zhao, S. Scott, X. Bao, *J. Energy Chem.*, 2013, **22**, 1-20.
4 J.J. Spivey, G. Hutchings, *Chem. Soc. Rev.*, 2014, **43**, 792-803.
5 L. Cornaglia, J. Munera, E. Lombardo, *Int. J. Hydrogen Energy*, 2015, **40**, 3423-3437.
6 F. Gallucci, E. Fernandez, P. Corengia, M.v.S. Annaland, *Chem. Eng. Sci.*, 2013, **92**, 40-66.
7 D. Mendes, A. Mendes, L.M. Madeira, A. Iulianelli, J.M. Sousa, A. Basile, *Asia-Pac. J. Chem. Eng.*, 2010, **5**, 111-137.
8 A.K. Kinage, R. Ohnishi, M. Ichikawa, *Catal. Lett.*, 2003, **88**, 199-202.
9 L. Wang, K. Murata, A. Sayari, B. Grandjean, M. Inaba, *Chem. Commun.*, 2001, 1952-1953.
10 O. Rival, B.P.A. Grandjean, C. Guy, A. Sayari, F. Larachi, *Ind. Eng. Chem. Res.*, 2001, **40**, 2212-2219.
11 F. Larachi, H. Oudghiri-Hassani, M.C. Iliuta, B.P.A. Grandjean, P.H. McBreen, *Catal. Lett.*, 2002, **84**, 183-192.
12 M.C. Iliuta, B.P.A. Grandjean, F. Larachi, *Ind. Eng. Chem. Res.*, 2003, **42**, 323-330.
13 Z. Liu, L. Li, E. Iglesia, *Catal. Lett.*, 2002, **82**, 175-180.
14 Z. Cao, H. Jiang, H. Luo, S. Baumann, W.A. Meulenberg, J. Assmann, L. Mleczko, Y. Liu, J. Caro, *Angew. Chem. Int. Ed.*, 2013, **52**, 13794-13797.
15 J.P. Tessonnier, B. Louis, M.J. Ledoux, C. Pham-Huu, *Catal. Commun.*, 2007, **8**, 1787-1792.
16 J.P. Tessonnier, B. Louis, S. Rigolet, M.J. Ledoux, C. Pham-Huu, *Appl. Catal. A*, 2008, **336**, 79-88.
17 B.D. Morreale, M.V. Ciocco, R.M. Enick, B.D. Morsi, B.H. Howard, A.V. Cugini, K.S. Rothenberger, *J. Membr. Sci.*, 2003, **212**, 87-97.
18 B.H. Howard, R.P. Killmeyer, K.S. Rothenberger, A.V. Cugini, B.D. Morreale, R.M. Enick, F. Bustamante, *J. Membr. Sci.*, 2004, **241**, 207-218.
19 G.J. Grashoff, C.E. Pilkington, C.W. Corti, *Platinum Metals Rev.*, 1983, **27**, 157-169.
20 A.L. Athayde, R.W. Baker, P. Nguyen, *J. Membr. Sci.*, 1994, **94**, 299-311.
21 R.C. Hurlbert, J.O. Konecny, *J. Chem. Phys.*, 1961, **34**, 655-658.
22 F. Roa, J.D. Way, *Ind. Eng. Chem. Res.*, 2003, **42**, 5827-5835.
23 K.S. Rothenberger, A.V. Cugini, B.H. Howard, R.P. Killmeyer, M.V. Ciocco, B.D. Morreale, R.M. Enick, F. Bustamante, I.P. Mardilovich, Y.H. Ma, *J. Membr. Sci.*, 2004, **244**, 55-68.
24 O. Camus, S. Perera, B. Crittenden, Y.C.v. Delft, D.F. Meyer, P.P.A.C. Pex, I. Kumakiri, S. Miachon, J.A. Dalmon, S. Tennison, P. Chanaud, E. Groensmit, W. Nobel, *AIChE J.*, 2006, **52**, 2055-2065.
25 L.S. McLeod, F.L. Degertekin, A.G. Fedorov, *J. Membr. Sci.*, 2009, **339**, 109-114.
26 R.E. Buxbaum, A.B. Kinney, *Ind. Eng. Chem. Res.*, 1996, **35**, 530-537.
27 S. Hara, A. Caravella, M. Ishitsuka, H. Suda, M. Mukaida, K. Haraya, E. Shimano, T. Tsuji, *J. Membr. Sci.*, 2012, **421-422**, 355-360.
28 G.S. Burkhanov, N.B. Gorina, N.B. Kolchugina, N.R. Roshan, *Platinum Metals Rev.*, 2011, **55**, 3-12.
29 A. Santucci, F. Borgognoni, M. Vadrucci, S. Tosti, *J. Membr. Sci.*, 2013, **444**, 378-383.
30 S. Uemiya, *Sep. Purif. Methods*, 1999, **28**, 51-85.
31 F.L. Chen, Y. Kinari, F. Sakamoto, Y. Nakayama, Y. Sakamoto, *Int. J. Hydrogen Energy*, 1996, **21**, 555-561.
32 S.H. Jung, K. Kusakabe, S. Morooka, S.D. Kim, *J. Membr. Sci.*, 2000, **170**, 53-60.
33 H. Abir, M. Sheintuch, *J. Membr. Sci.*, 2014, **466**, 58-69.
34 B.M. Weckhusen, D. Wang, M.P. Rosynek, J.H. Lunsford, *J. Catal.*, 1998, **175**, 338-346.
35 D. Ma, Y. Shu, M. Cheng, Y. Xu, X. Bao, *J. Catal.*, 2000, **194**, 105-114.
36 W. Li, G.D. Meitzner, R.W.B. III, E. Iglesia, *J. Catal.*, 2000, **191**, 373-383.
37 H. Aritani, H. Shibasaki, H. Orihara, A. Nakahira, *J. Environ. Sci.*, 2009, **21**, 736-740.

38 D. Wang, J.H. Lunsford, M.P. Rosynek, *Top. Catal.*, 1996, **3**, 289-297.
39 A. Sarioglan, O.T. Savasci, A.E. Senatalar, A. Tuel, G. Sapaly, Y.B. Taarit, *J. Catal.*, 2007, **246**, 35-39.
40 D. Wang, J.H. Lunsford, M.P. Rosynek, *J. Catal.*, 1997, **169**, 347-358.
41 Y. Shu, D. Ma, L. Xu, Y. Xu, X. Bao, *Catal. Lett.*, 2000, **70**, 67-73.
42 C.L. Zhang, S. Li, Y. Yuan, W.X. Zhang, T.H. Wu, L.W. Lin, *Catal. Lett.*, 1998, **56**, 207-213.
43 P.L. Tan, Y.L. Leung, S.Y. Lai, C.T. Au, *Appl. Catal. A*, 2002, **228**, 115-125.
44 V. Abdelsayed, D. Shekhawat, M.W. Smith, *Fuel*, 2015, **139**, 401-410.
45 K. Honda, X. Chen, Z.G. Zhang, *Appl. Catal. A*, 2008, **351**, 122-130.
46 S. Kikuchi, R. Kojima, H. Ma, J. Bai, M. Ichikawa, *J. Catal.*, 2006, **242**, 349-356.
47 C.H. Bartholomew, *Appl. Catal. A*, 2001, **212**, 17-60.
48 Z. Liu, M.A. Nutt, E. Iglesia, *Catal. Lett.*, 2002, **81**, 271-279.
49 R. Kojima, S. Kikuchi, H. Ma, J. Bai, M. Ichikawa, *Catal. Lett.*, 2006, **110**, 15-21.
50 H. Ma, R. Ohnishi, M. Ichikawa, *Catal. Lett.*, 2003, **89**, 143-146.
51 A.C.C. Rodrigues, J.L.F. Monteiro, *Catal. Commun.*, 2008, **9**, 1060-1065.
52 M.R. Toosi, B. Sabour, T. Hamuleh, M.H. Peyrovi, *Reac. Kinet. Mech. Cat.*, 2010, **101**, 221-226.
53 A. Haken, F. Roessner, W. Reschetilowski, *Chem. Eng. Technol.*, 1995, **18**, 414-419.
54 G. Chiappetta, G. Barbieri, E. Drioli, *Chem. Eng. Proc.*, 2010, **49**, 722-731.
55 S. Liguori, A. Iulianelli, F. Dalena, V. Piemonte, Y. Huang, A. Basile, *Int. J. Hydrogen Energy*, 2014, **39**, 18702-18710.
56 Y.H. Kim, R.W.B. III, E. Iglesia, *Microporous Mesoporous Mater.*, 2000, **35-36**, 495-509.
57 F. Solymosi, J. Cserenyi, A. Szoke, T. Bansagi, A. Oszko, *J. Catal.*, 1997, **165**, 150-161.
58 H. Liu, X. Bao, Y. Xu, *J. Catal.*, 2006, **239**, 441-450.
59 B.S. Liu, L. Tian, L. Li, C.T. Au, A.S.C. Cheung, *AIChE J.*, 2011, **57**, 1852-1589.
60 H. Liu, W. Shen, X. Bao, Y. Xu, *Appl. Catal. A*, 2005, **295**, 79-88.
61 B.M. Weckhusen, D. Wang, M.P. Rosynek, J.H. Lunsford, *J. Catal.*, 1998, **175**, 347-351.
62 Y. Song, Y. Xu, Y. Suzuki, H. Nakagome, Z.G. Zhang, *Appl. Catal. A*, 2014, **482**, 387-396.
63 P.L. Tan, C.T. Au, S.Y. Lai, *Catal. Lett.*, 2006, **112**, 239-245.
64 D. Ma, D. Wang, L. Su, Y. Shu, Y. Xu, X. Bao, *J. Catal.*, 2002, **208**, 260-269.
65 J.B. Claridge, A.P.E. York, A.J. Brungs, C. Marquez-Alvarez, J. Sloan, S.C. Tsang, M.L.H. Green, *J. Catal.*, 1998, **180**, 85-100.
66 E.V. Fadeeva, O.P. Tkachenko, A.V. Kucherov, A.P. Barkova, M.N. Mikhailov, A.M. Kuli-Zade, M.K. Akhmedov, L.M. Kustov, *Russ. Chem. Bull.*, 2012, **61**, 2230-2335.
67 O. Bayraktar, E.L. Kugler, *Appl. Catal. A*, 2002, **233**, 197-213.
68 J. Bai, S. Liu, S. Xie, L. Xu, L. Lin, *Catal. Lett.*, 2003, **90**, 123-130.
69 Y. Li, L. Liu, X. Huang, X. Liu, W. Shen, Y. Xu, X. Bao, *Catal. Commun.*, 2007, **2007**, 1567-1572.
70 W. Ding, S. Li, G.D. Meitzner, E. Iglesia, *J. Phys. Chem. B*, 2001, **105**, 506-513.
71 D. Ma, Y. Lu, L. Su, Z. Xu, Z. Tian, Y. Xu, L. Lin, X. Bao, *J. Phys. Chem. B*, 2002, **106**, 8524-8530.
72 R. Ohnishi, S. Liu, Q. Dong, L. Wang, M. Ichikawa, *J. Catal.*, 1999, **182**, 92-103.
73 M.C.J. Bradford, M. Te, M. Konduru, D.X. Fuentes, *Appl. Catal. A*, 2004, **266**, 55-66.
74 M.C. Iliuta, F. Larachi, B.P.A. Grandjean, I. Iliuta, *Ind. Eng. Chem. Res.*, 2002, **41**, 2371-2378.

Palladium membrane reactors significantly improve C_6H_6 yield from CH_4 dehydroaromatization on Mo/HZSM-5 catalysts over a wide range of space velocity.